7 Interaction between a Wildfire and the Sea-Breeze Front

Deborah E. Hanley
AWS Truepower, LLC, 463 New Karner Road, Albany, NY 12205, USA
Email: dhanley@awstruepower.com Phone: 518-213-0044 X 1027

Philip Cunningham
Earth and Environmental Sciences Division, Los Alamos National Laboratory,
Los Alamos, New Mexico 87545, USA
Email: pcunning@lanl.gov Phone: 505-667-5092

Scott L. Goodrick
Center for Forest Disturbance Science, USDA Forest Service,
Athens, Georgia 30602, USA
Email: sgoodrick@fs.fed.us Phone: 706-559-4237

Abstract Florida experiences sea breezes, lake breezes, and bay breezes almost every day during the year, and there are frequently complex interactions between many of these breezes. Given the often-rapid changes in temperature, humidity and wind speed that accompany these breezes, most wildfires and prescribed fires in Florida are affected in some way by their interaction with these circulations. In this paper, we explore the interaction between sea breezes and wildland fires from both an observational and an idealized modeling perspective. The progression of the sea-breeze front and its interaction with the smoke plume from a 26,000 acre wildfire are tracked using a variety of data sources including surface and upper-air observations as well as NEXRAD radar imagery. Idealized numerical simulations of a thermally buoyant plume interacting with a density current are performed in an effort to enhance our understanding of the dynamics of the interaction between sea breeze circulations and the convective column of the fire. Our observational analysis and idealized modeling results suggest that the arrival of a sea breeze front induces a temporary, but significant, increase in fire intensity. This intensification precedes the arrival of the sea-breeze front at the location of the fire, such that the fire intensity is at a maximum at the time of, and slightly after, the passage of the front, and decreases gradually thereafter as cooler and moister air behind the front arrive.

Keywords Sea-breeze, fire behavior, fire weather, numerical modeling

7.1 Introduction

Weather is one of the most important factors leading to extreme wildfire behavior. Rapid changes in wind can quickly affect the rate and direction of fire spread, and may have a significant impact on fire intensity. Changes in temperature and humidity also may cause unexpected changes in fire behavior. Florida coastlines experience sea-breezes, lake breezes, and bay breezes almost every day during the year, and there are frequently complex interactions between many of these breezes. Given the often-rapid changes in temperature, humidity and wind speed that accompany these breezes, most wildfires in Florida are affected in some way by their interaction with these circulations. Nevertheless, despite the importance of sea-breeze circulations for fire behavior, the nature of the interaction between sea-breezes and wildfires remains relatively poorly understood.

Previous studies of sea-breezes depended upon a network of observation sites in the area of the sea-breeze (e.g., Atkins and Wakimoto, 1997), or used numerical models to simulate the sea-breeze (e.g., Pielke, 1974; Sha et al., 1991; Rao et al., 1999; Colby, 2004). Radar and satellite imagery have been shown to be useful in tracking the structure, evolution and timing of the movement of sea-breeze fronts (e.g., Atlas, 1960; Wakimoto and Atkins, 1994; Atkins et al., 1995; Atkins and Wakimoto, 1997), and have also been used to observe smoke plumes from fires (e.g., Banta et al., 1992; Rogers and Brown, 1997; Hufford et al., 1998), as well as from other sources of particulate emissions such as volcanoes, dust storms, and industrial emissions.

In this Chapter, we explore the interaction between sea-breezes and wildfires in more detail from both an observational and an idealized modeling perspective. The progression of the sea-breeze front and its interaction with the smoke plume from the fire are tracked using a variety of data sources including surface observations from the remote automated weather station (RAWS) network, surface and upper-air observations from the national oceanic and atmospheric administration/national weather service (NOAA/NWS), and imagery from the Weather Surveillance Radar-1988 Doppler (WSR-88D) site in Tallahassee, Florida. Given that the sea-breeze may be represented by a density current, idealized numerical simulations of a thermally buoyant plume interacting with a density current are performed in an effort to enhance our understanding of the dynamics of the interaction between sea-breeze circulations and smoke plumes. Although these idealized simulations do not allow us to determine directly the impact of the sea-breeze on fire behavior, which would require a fully coupled atmosphere–fire model (e.g., Clark et al., 1996ab, 2004; Linn, 1997; Linn and Cunningham, 2005), they do provide insight into the interpretation of fire behavior observations, and allow us to make inferences as to how the fire behavior would likely change in response to the simulated changes in atmospheric circulations. The combination of observations, idealized modeling results and inferences on fire behavior lead

to the development of an initial conceptual model of how the sea-breeze impacts wildfire behavior.

7.1.1 Sea-Breeze Structure and Characteristics

Simpson (1994) provides a detailed overview of the structure and evolution of the sea-breeze front derived from observations as well as numerical and laboratory studies. It is generally observed that the development of the sea-breeze is dependent both upon the temperature difference between the land and the adjacent water surface and upon the strength of any prevailing offshore winds. Offshore flow can often have a dramatic effect on the depth of the sea- breeze circulation. The depth of the sea-breeze circulation may be less than 50 m with winds above this level blowing in the opposite direction. As time progresses, the depth of the sea breeze may reach 1,000 m or more.

The inland penetration of the sea-breeze can vary from 30 – 300 km depending upon the location. Typical distances in Florida are about 50 km, although strong prevailing winds that are in the same direction as the sea-breeze can often result in much deeper penetration, almost to the opposite coast. Florida also has a unique geographic design, being surrounded by water on the east and west coast of the peninsula as well as along the Panhandle coastline. Sea-breezes are observed along all the coasts as well as along the bays, inlets and large lakes like Lake Okeechobee in central Florida. These lake and bay breezes interact with the coastal sea-breezes and result in very complicated wind patterns. Forecasting the winds associated with the sea-breeze passage is also made more difficult by the presence of convex and concave coastlines, resulting in additional convergence and divergence effects (Simpson et al., 1977).

Wakimoto and Atkins (1994) and Atkins and Wakimoto (1997) showed that there were significant differences between the sea-breezes observed under offshore and onshore flow conditions. The offshore flow case exhibited stronger low-level convergence, larger vertical velocities, and higher radar reflectivity values at the sea-breeze front, also known as a radar thin line. The sea-breeze thin line and the kinematic sea-breeze frontal boundary are found to be co-located and easily identifiable on offshore flow days. Onshore flow days typically have a much weaker front and the radar thin line is often hard to detect. In the offshore flow case, the radar thin line is found to increase in intensity during the day and gradients of temperature and moisture are strongest on these days.

It is generally accepted that sea-breeze circulations are dynamically similar to density currents (e.g., Simpson, 1994), which are predominantly horizontal flows driven by density differences. Atkins et al. (1995) note that in the case of an offshore flow sea-breeze, there was a kinematic frontal structure similar to that found in density currents produced in the laboratory. Wakimoto and Atkins (1994) calculated the speed of sea-breeze fronts and found them to be closely matched

to the theoretical speeds of comparable density currents. Further study by Atkins and Wakimoto (1997) showed Froude numbers for offshore and parallel flow sea-breeze events, as well as for gust fronts, compared well to values calculated from laboratory density current experiments. This comparison was not as well defined on the onshore flow days where the sea-breeze was moving slower than would be expected using density current theory. It is not clear why this discrepancy exists for onshore flow sea-breezes, although it is suggested that it may be related to the difficulty in locating the location of the frontal zone in these cases.

7.1.2 Radar Observations of Smoke Plumes and the Sea-Breeze

Many wildfires occur in remote regions where observations are limited; as a result, the use of satellite and radar imagery is becoming more prominent in fire detection and monitoring. It has been suggested that remotely sensed data might also be useful in fire behavior prediction (Hufford et al. 1998). Both smoke plumes from fires (e.g., Banta et al., 1992) and sea-breeze fronts (e.g., Wilson et al., 1994) are clearly visible on radar, especially when the radar is in clear-air mode.

Previous studies of the signals returned from the radar during clear-air mode operation have suggested that the echoes are most likely that of birds or insects (Crawford, 1949; Hardy and Katz, 1969; Wilson et al., 1994). Wilson et al. (1994) found that the thin line echoes commonly seen in association with sea-breezes correlated to updraft regions and result from insects actively flying downward to avoid being carried to colder regions of the atmosphere. Atlas (1960) discounts the idea of echoes resulting from birds or insects since they would have to fly along in a very narrow beam, lowering their flight as the beam lowered, or fly in broad waves normal to the beam with the same speed as the beam. Instead, Atlas suggests the pattern seen is a result of a sharp increase in the refractive index. The contrast on the radar is highest when the offshore flow is dry so the contrast is high, leading to higher refractive discontinuities. This would require a sharp vertical lapse rate. Battan (1973) suggests both insects and refractive gradients could be responsible for the radar echoes. Despite some uncertainty regarding exactly what causes the echoes, the sea-breeze signature is readily apparent on the radar for the present case and can be used to follow the inland propagation of the sea-breeze front.

Plumes of smoke have also been observed using radar and satellite imagery in remote locations such as Alaska (Hufford et al., 1998), where plumes from a large wildfire were readily apparent on radar. The plumes from smaller fires were not visible, and it was suggested that the plumes in these cases were concentrated below the level of the radar beam. High reflectivities (i.e., $20-25$ dBZ) were noted near the head of the fire, however, and Hufford et al. (1998) suggested that radar imagery can be used to provide information on fire location, intensity and growth, smoke plumes and fire weather.

Smoke from a major industrial fire in Montreal, Canada, was observed on three radars operated by McGill University on 23 May 1996 (Rogers and Brown, 1997). They suggested that fires produce particulate matter (PM) and create fluctuations in the refractive index, both of which are potentially detectable by the radar. In this case, they concluded that the echoes are the result of scattering by the particles. Banta et al. (1992) also support the idea that particles in smoke are responsible for the echoes, with the particles having a flat or needle shape (ash platelets or pine needles).

7.1.3 Effect of Sea-Breezes on Fires

There are three main factors that affect fire behavior: fuel, weather and topography. Weather is by far the most variable and arguably the most important of the three. Wind is a strong driver of the rate and direction of fire spread and can also alter fire intensity as well. Changes in wind direction can transform a low intensity backing fire (moving into the wind) or a moderate intensity flanking fire (moving laterally to the wind) into an intense head fire (moving with the wind) capable of overrunning fire fighters who thought they were located in a safe area.

Firefighters typically monitor weather conditions regularly for any changes in wind speed or direction at the scene of the fire using hand-held instruments or portable weather stations. On days where there is adequate moisture, a line of approaching clouds and a gust front may indicate the approach of the sea-breeze front. On dry days, there may be no clouds to warn of the impending frontal passage and the first indication may be the arrival of the gust front. Most fire personnel do not have direct access to radar or satellite data while on a fire scene. Local knowledge of the behavior of the sea breeze is extremely important on both wildfires and prescribed fires as the onset and structure of the sea breeze are typically highly regular in Florida in spring and summer months. One case of a springtime wildfire that is of interest is the East fork fire because of the array of data that was available during the incident and the opportunity it provided to study the sea-breeze–wildfire interaction in a novel way.

7.1.4 East Fork Fire

The East fork fire began either late on 4 April 2004, or early on 5 April 2004, in the Bradwell Bay Wilderness area of the Apalachicola national forest. This area is located in the Florida Panhandle, just southwest of Tallahassee. It is believed that the fire was human-caused, either arson or accidental. The fire ultimately burned over 26,000 acres of the wilderness area. Fire fighting was made difficult due to the restriction on the use of heavy equipment in the wilderness area itself. The fire was considered 90% contained by April 16, 2004.

The sea-breeze was a major factor in fighting the East fork fire. Winds shifted direction on most afternoons, and these wind shifts resulted in varying directions of fire spread. Firefighters had to be aware of these possible weather changes and be able to adjust tactics as the weather changed. Conditions during this period were generally dry, and the daily sea-breeze circulations did not bring any beneficial rains and for the most part were dry events. Because of the dry conditions, the WSR-88D radar site in Tallahassee was operating in clear-air mode at the time of the fire. During clear-air mode periods, the sea-breeze front is often clearly visible on the radar; moreover, smoke plumes can often be seen if they are close enough to the radar. In this case, both the sea-breeze and the smoke plume were noted together and the resulting interaction between the plume and the sea-breeze front could be observed.

The plan of the present Chapter is as follows: in the following section, the data and methodology for both the case study and the idealized numerical simulations are described, while Section 7.3 presents the results of the case study. In Section 7.4, idealized numerical simulations are presented that explore the interaction between a buoyant plume and a density current, and Section 7.5 summarizes the main results of the present investigation and presents a conceptual model for sea-breeze–fire interactions.

7.2 Data and Methodology

7.2.1 Case Study

The goal of this study is to provide an improved understanding of the interactions between wildfires and sea-breeze circulations. The foundation of this understanding is based upon specific observations of one event that will be augmented by idealized numerical simulations. The atmospheric component can be adequately described through a combination of surface observations, upper-air soundings and radar data (both base reflectivity and radial velocity). Description of the fire is considerably more problematic, as no direct measurements of the fire are available, except for daily estimates of area burned. As an alternative, we focus on the behavior of the smoke plume as observed by the Tallahassee WSR-88D radar as a surrogate, since Hufford et al. (1998) found high reflectivities to be associated with more intense burning.

The East Fork Fire burned over a period of approximately two weeks in early April of 2004; however, this study only focuses on the early stages of the fire, specifically the afternoon of April 5. The location of the East fork fire and the four nearby weather stations are shown in Fig. 7.1. Observations of temperature, relative humidity, wind speed and direction are used to track the passage of the sea-breeze front. A high-pass filter was applied to the temperature and relative

humidity time series to remove waves with periods greater than or equal to 24 h. The high-pass filter was accomplished using a Fourier decomposition of a 96 h time series for each station and recomposing the time series with the longer wave periods excluded.

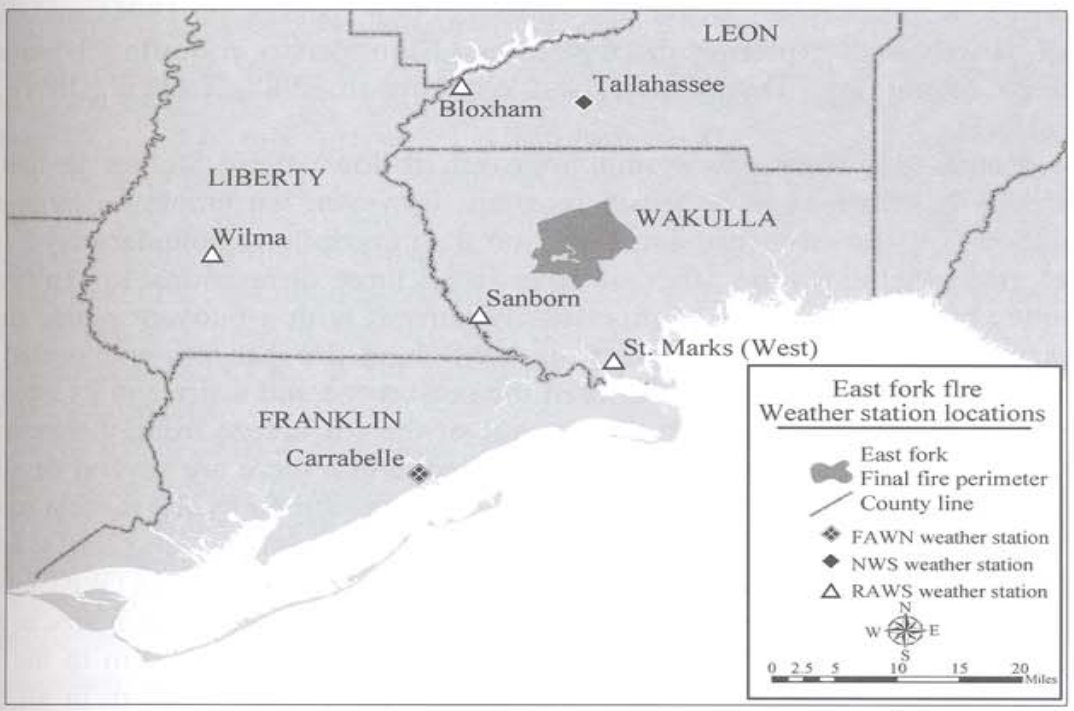

Figure 7.1 Fire perimeters and observation locations

As noted above, the Tallahassee WSR-88D radar was operating in clear-air mode during this period, which is its most sensitive mode of operation (Crum and Alberty, 1993). The antenna has a slower rotation rate than in precipitation mode that increases the radar sensitivity, and therefore its ability to sense smaller objects in the atmosphere. Most of the signal in this mode will be the result of airborne dust and PM. In this mode, the radar scans five different elevation angles (0.5° – 4.5°, in 1° increments) and takes about 10 minutes to complete each scan. In this study we will focus our attention on the three lowest elevations (0.5°, 1.5°, and 2.5°) of the base reflectivity and radial velocity fields.

7.2.2 Idealized Numerical Simulations

The sea-breeze has been studied extensively in the past, and many studies have involved the use of numerical models to simulate sea-breeze circulations, both in an effort to simulate observed cases and in an idealized context to explore their structure and dynamics. From the perspective of idealized simulations of the

sea-breeze, Dailey and Fovell (1999), Fovell and Dailey (2001), and Fovell (2005) used a 3D cloud-resolving numerical model with horizontal resolutions as high as 500 m to explore various aspects of the interactions between sea-breeze fronts and horizontal convective rolls in the boundary layer. Several investigators have employed even higher resolution in 2D configurations to explore the parallel between sea-breeze fronts and density currents (e.g., Sha et al., 1991), and in this regard, simulations exploring the dynamics of thunderstorm outflow boundaries are also relevant (e.g., Droegemeier and Wilhelmson, 1987; Xu et al., 1996; Xue et al., 1997).

As discussed further below, our approach follows these studies in that the sea-breeze is idealized as a density current; however, we employ a large-eddy simulation (LES) model focusing solely on the atmospheric boundary layer, with model grid spacing on the order of 10 m in all three dimensions, to explore the dynamics of the interaction of this density current with a buoyant plume that is representative of the smoke plume from a wildland fire. Since it is expected that the most significant interaction between the sea-breeze and a fire and its attendant plume will occur primarily with the passage of the sea-breeze front, this approach appears to be justified, although we acknowledge that there are several details of observed sea-breeze circulations that cannot be represented by the present model.

The LES model to be used is described by Cunningham et al. (2005), and is based on the dynamical core of the weather research and forecasting (WRF) model in physical height coordinates (Skamarock et al., 2001). The domain size used in these simulations is a rectangular box of size $800 \times 3{,}200 \times 1{,}000$ m in the x, y, and z directions, respectively, with a uniform grid spacing of 10 m in all three directions. Boundary conditions are periodic in the x-direction and open-radiative in the y-direction. Other details of the LES model are identical to those described by Cunningham et al. (2005).

As noted previously, there is significant evidence that a sea-breeze front can be interpreted as a density current, particularly when the ambient wind is in the offshore direction. Density currents have been explored extensively by numerical models, in an atmospheric context primarily in connection with thunderstorm outflows (e.g., Droegemeier and Wilhelmson, 1987; Xu et al., 1996; Xue et al., 1997), but also in oceanographic (e.g., Özgökmen et al., 2004) and general fluid mechanics (e.g., Härtel et al., 2000) contexts, and even with respect to the backdraft phenomenon in building fires (e.g., Fleischmann and McGrattan, 1999). Here we initialize the density current with a cold pool that is uniform in the y-direction in the presence of an opposing flow, to simulate the advance of a sea-breeze front in the presence of offshore winds.

As a final comment concerning the modeling approach, we emphasize that the goal of the idealized modeling portion of this study is not to reproduce the behavior in the observed case, but rather to gain insight into the basic dynamical processes associated with the interaction between a sea-breeze front and a buoyant plume representative of those seen with wildland fires.

7.3 Case Study Analysis

The East fork fire began late on April 4, 2004, or early on April 5, 2004, and is suspected to have been started by human causes, either accidental or arson. The fire burned in timber and southern rough fuel groups. According to the National Interagency Coordination Center reports, by April 7 the fire reached 7,000 acres (28.3 km^2) and was only 20% contained. Spotting of up to 0.25 mile (0.4 km) ahead of the main fire front was observed with rates of spread of 20 – 30 chains per hour (0.11 – 0.17 $m \cdot s^{-1}$) reported. This observed fire activity continued and by April 8, the area burned had increased to over 8,400 acres (34.0 km^2). By April 13, the fire had consumed almost 20,000 acres (80.9 km^2) and was only 70% contained. The fire ultimately consumed over 26,000 acres (105.2 km^2) of wilderness area and was 90% contained by April 15. The total area burned was increased by back burning activities of the fire suppression crews. Back burning is used to remove fuels ahead of the active fire front and impede the spread of the fire and help in containment.

Hourly surface observations were used to provide an estimate of the passage of the sea-breeze front. Unfiltered time series of temperature and relative humidity data from four stations near the fire (not shown) indicate that Sanborn, the closest of the four stations to the coast, shows the earliest peak in temperature (1,400 EDT), while the peak at the other stations is delayed by approximately 2 h. Following the temperature maximum is a decrease in temperature spanning 6 – 8 h, which is hardly indicative of the passage of the sea-breeze front, and more closely resembles the normal diurnal cycle. The unfiltered relative humidity time series does not show a marked change in air mass either. Using a high-pass filter to remove the diurnal signal as described in the previous section reveals a stronger sea-breeze signal in both the temperature and relative humidity time series (Fig. 7.2). It is apparent that Sanborn shows the earliest start to humidity recovery around 1,700 EDT with the other stations following rather sharply an hour later.

The sea-breeze front can be seen clearly on the Tallahassee 0.5° elevation base reflectivity imagery at 1828 UTC (Fig. 7.3). The East Fork Fire is visible approximately 40 km southwest of the radar location and is indicated by a reflectivity of approximately 18 dBZ with the smoke plume traveling toward the southeast (Fig. 7.3(a)). The sea-breeze front continues to move inland over the next several hours and by 1927 UTC (Fig. 7.3(b)) the smoke plume from the fire can be seen to increase in intensity with reflectivities reaching 28 – 32 dBZ for a brief period prior to the arrival of the sea-breeze front. By 2025 UTC the sea-breeze is just reaching the fire and the plume is displaying reflectivities in the range of 20 – 25 dBZ near the fire (Fig. 7.3(c)), consistent with values observed by Hufford et al. (1998) near the head of a rapidly moving wildfire. At 2124 UTC, the sea-breeze front has reached the fire, as evidenced by the humidity recovery indicated by the Sanborn RAWS site. Despite the start of humidity recovery the

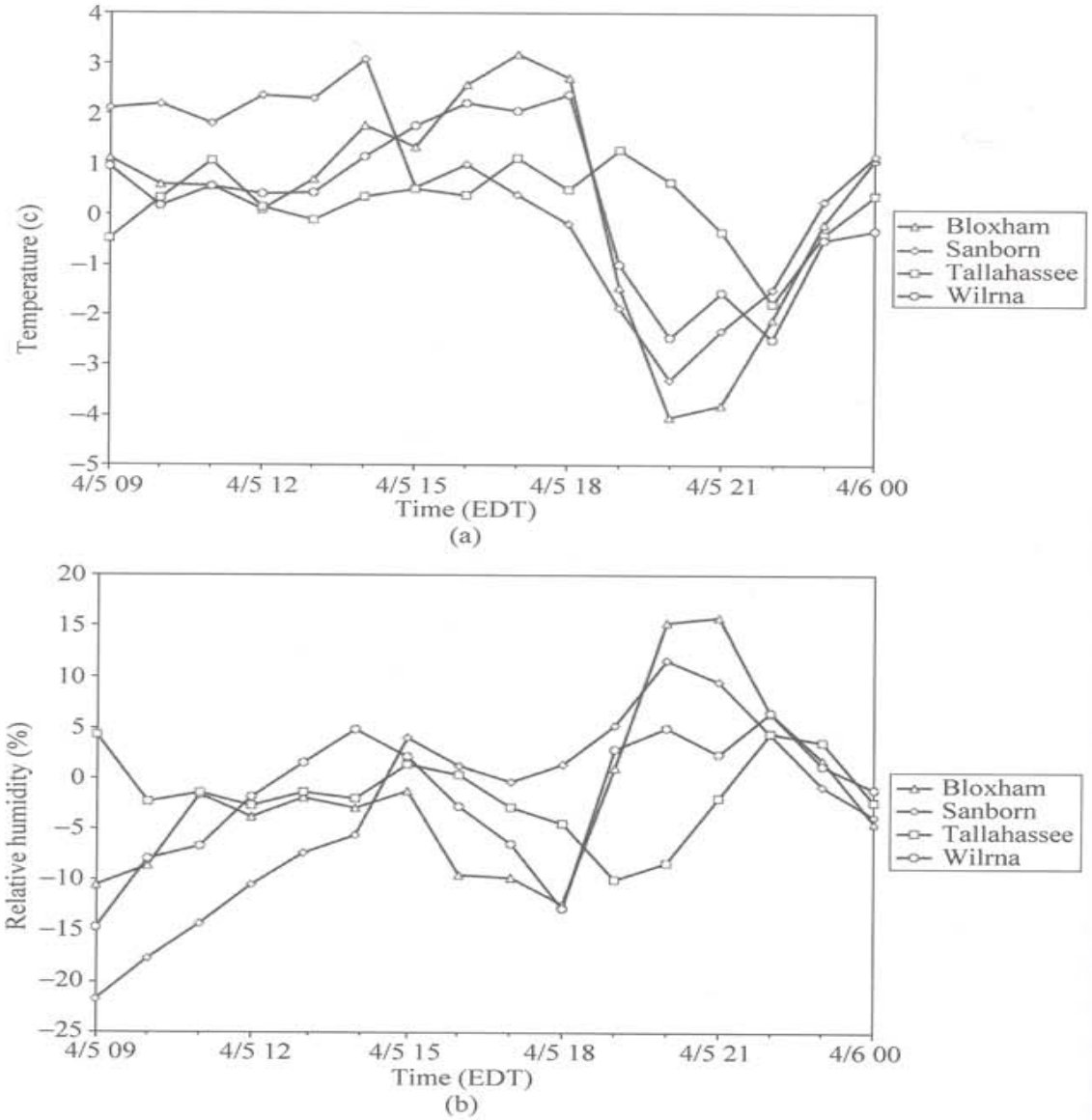

Figure 7.2 High-pass filtered time series of (a) temperature and (b) relative humidity at the surface for the period starting at 0900 EDT 5 April 2004 and ending at 0000 EDT 6 April 2004, for several stations identified in Fig. 7.1

plume intensifies to levels not previously seen with a large core of the plume now displaying reflectivities in the 28 – 32+ dBZ range (Fig. 7.3(d)). Upper-level winds at this time are carrying the plume back toward the coast, aided by the upper-level return flow of the sea-breeze circulation. The reflectivity of the plume decreases from this peak over the next several hours as the fire begins to respond to the decreased temperature and increased moisture of the marine air, leading to a decline in fire intensity (Figs. 7.3(e) and (f)).

Base reflectivities from the 0.5°, 1.5° and 2.5° elevations are used to examine the vertical structure of the plume at 2,124 UTC, the time of greatest intensity

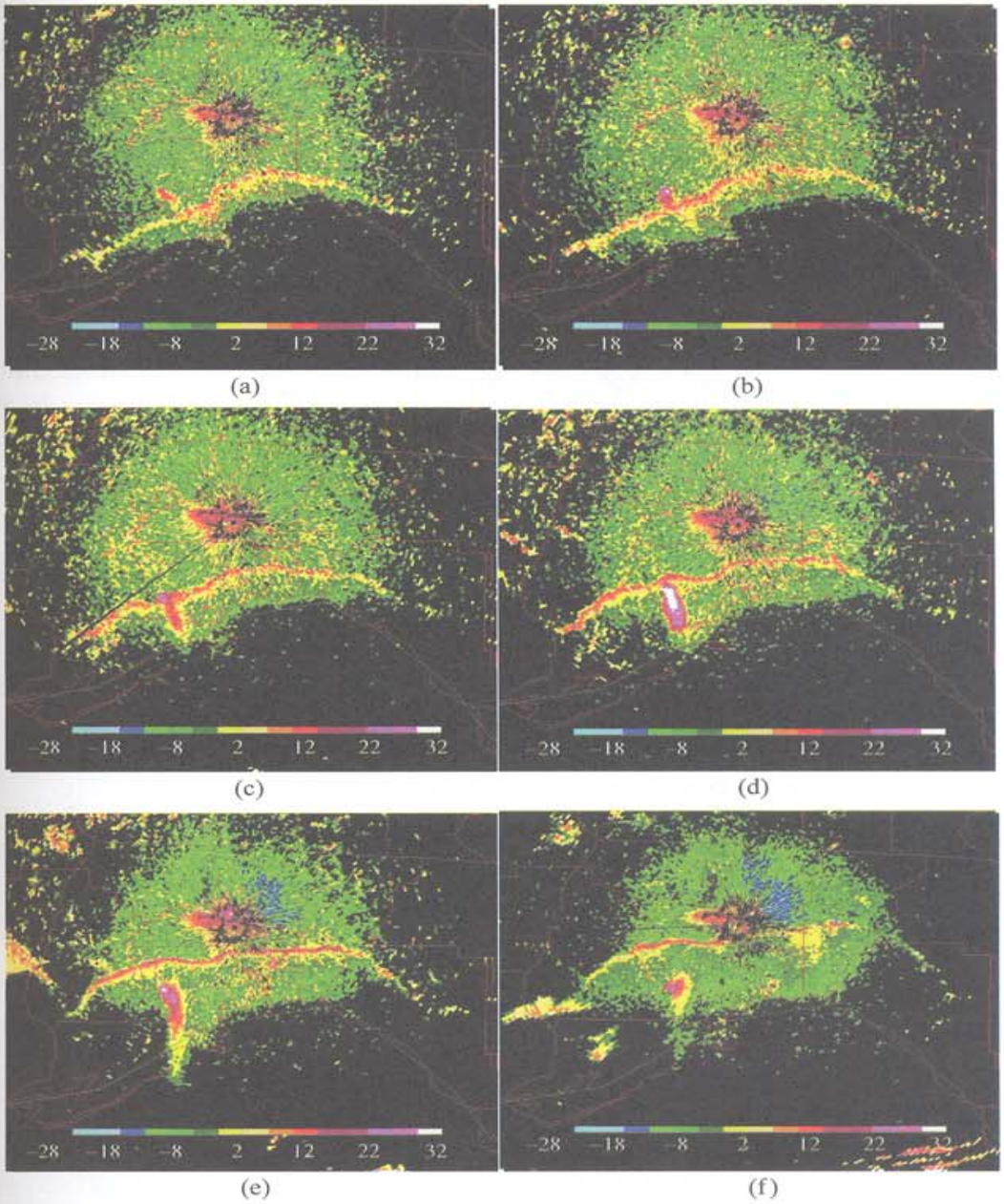

Figure 7.3 Radar reflectivity (dBZ, shaded as indicated) at a scan elevation of 0.5° at (a) 1828 UTC, (b) 1927 UTC, (c) 2025 UTC, (d) 2124 UTC, (e) 2223 UTC, and (f) 2323 UTC for 5 April 2004

(Fig. 7.4). At the lowest elevation, the overall plume is 21.25 km in length with the region of reflectivity >28 dBZ having a length of 8.75 km. The approximate heights of the centroids of the ends of the plume at this elevation are 453 m and 638 m, well within the 800 m deep mixed layer (estimated from the 1200 UTC sounding and observed high temperature). At the 1.5° elevation, the plume is

slightly longer, 23.75 km (length of the 28+ dBZ core has shrunk to 3.75 km), ranging in height from 1,151 – 1,637 m. At this elevation the plume is clearly above the mixed layer and in the return flow of the sea-breeze circulation. The 2.5° elevation reveals a considerably smaller plume, 8.75 km in length (2.5 km for the 28+ dBZ core), and spanning elevations of 1,849 – 2,157 m. The northwest corners of the plumes at each level are collocated, indicating that the plume has a rather strong vertical core immediately above the fire that would be consistent with an intensely burning fire producing a strong buoyancy flux.

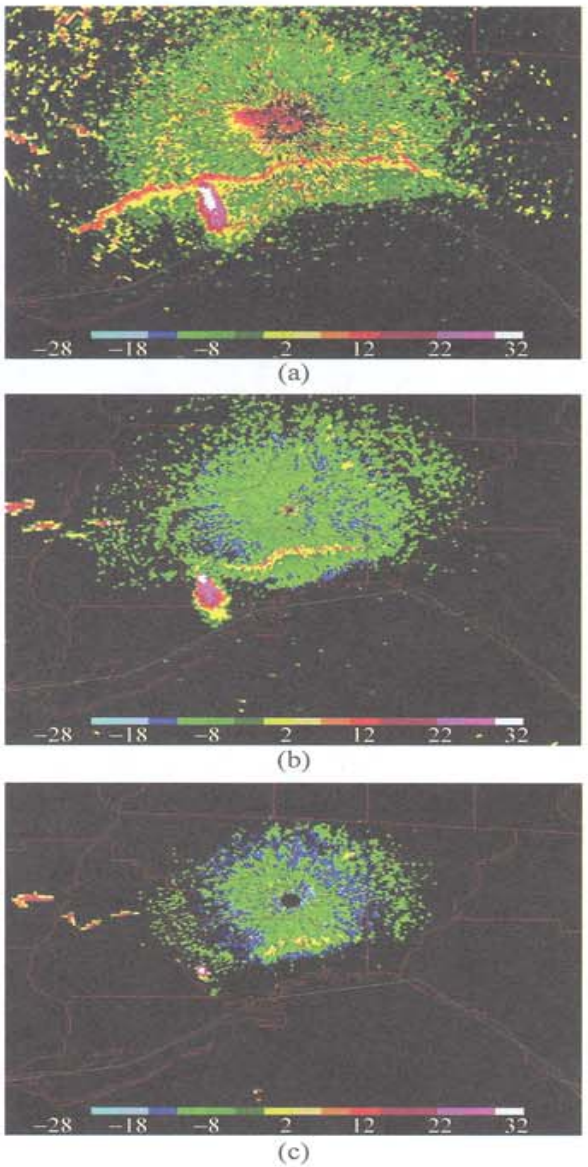

Figure 7.4 Radar reflectivity (dBZ, shaded as indicated) at 2124 UTC for 5 April 2004 at scan elevations of (a) 0.5°, (b) 1.5°, and (c) 2.5°

The radial velocity field from the WSR-88D is a useful tool in identifying areas of convergence and divergence. The 0.5° elevation radial velocity field from Tallahassee shows a well defined convergence zone along the sea-breeze front as it pushes inland against the prevailing northwesterly flow in the region (Fig. 7.5). Near the fire the pattern is more complex as the rising plume generates a region of divergence oriented along the axis of the plume, possibly marking the return flow of the thermal circulation generated by the intense heating of the fire. At the 1.5° elevation, a divergence pattern is still discernible along the plume axis although its extent is limited to the area near the peak in base reflectivity.

It should be noted that we have avoided making any direct comments as to the magnitudes of the velocities shown. This is due to the relatively broad spectrum width observed by the radar in the vicinity of the plume which is indicative of a highly turbulent environment, and thus renders the magnitudes of the radar-derived velocities less reliable.

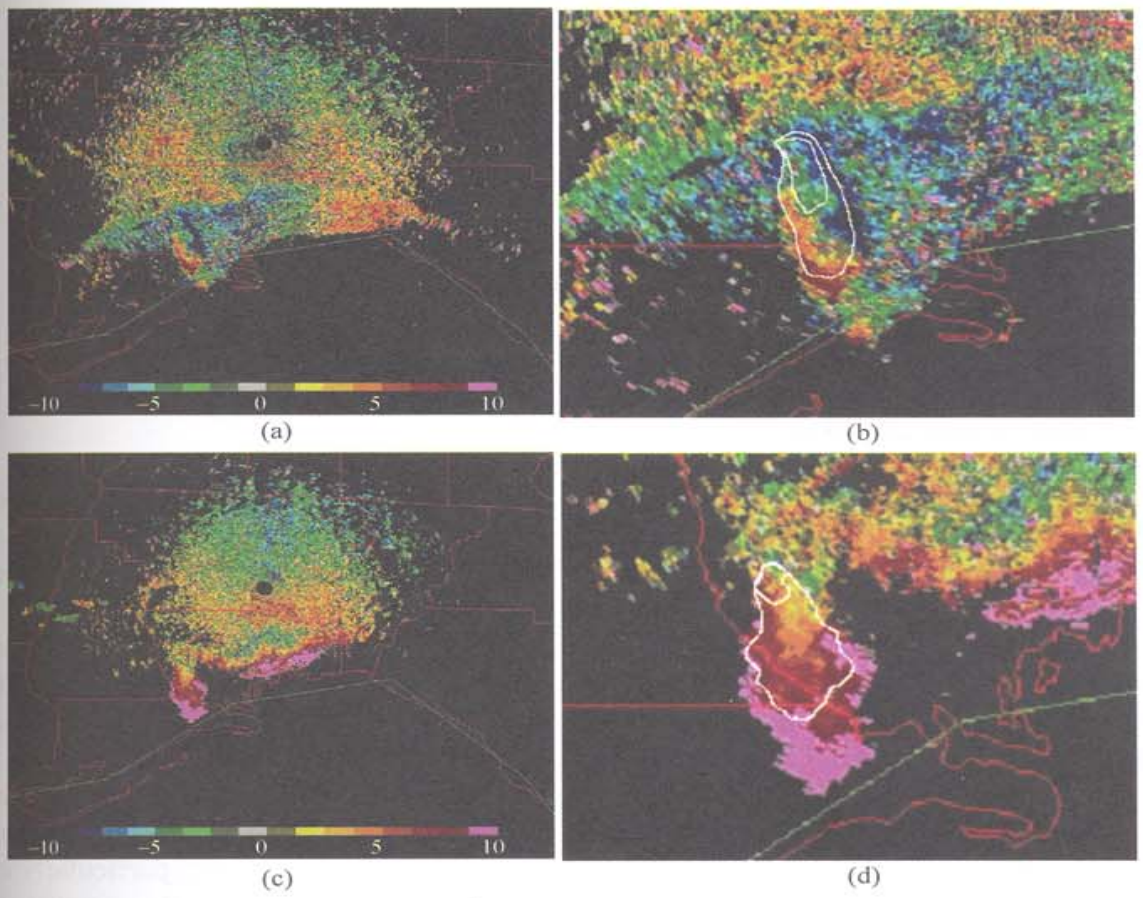

Figure 7.5 Radial velocity ($m \cdot s^{-1}$, shaded as indicated) at 2,124 UTC for 5 April 2004 at scan elevations of (a) 0.5° and (c) 1.5°. Panels (b) and (d) provide close-up representations of panels (a) and (c), respectively, with base reflectivities of 12 dBZ and 28 dBZ indicated by the solid contours

7.4 Numerical Simulations

In this Section, we present results from three numerical simulations to explore the nature of the interaction between a density current and a buoyant plume: two simulations in which a density current and a plume are examined in isolation, respectively, and one in which both are present and are allowed to interact.

The density current is initialized with a cold pool at one end of the domain (Fig. 7.6). When the simulation is started, the cold pool adjusts under gravity and initiates a density current that travels in the positive y-direction. The ambient winds are directed in the negative y-direction, thus representing an offshore flow situation. The cold pool is initially uniform in the x-direction, but rapidly becomes 3D with the development of lobe and cleft instabilities (not shown), consistent with laboratory experiments and previous numerical investigations using three-dimensional models.

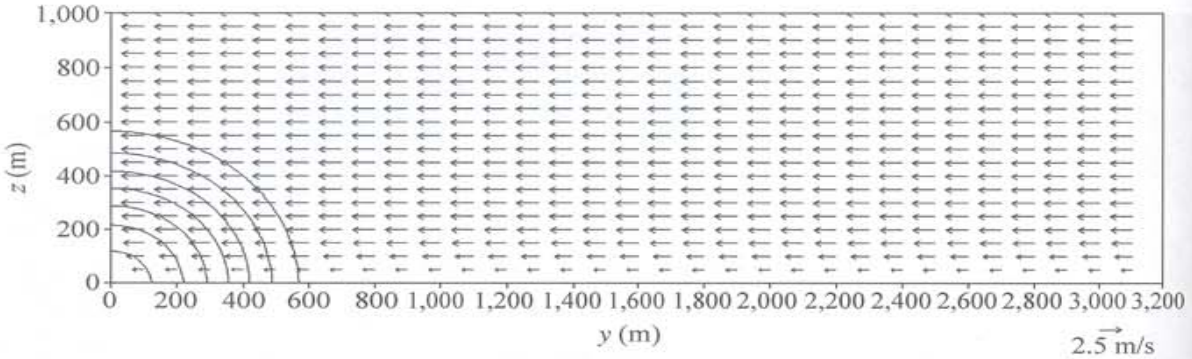

Figure 7.6 Model initial conditions in the $y-z$ plane at $x=480$ m of potential temperature (contour interval 1 K) and wind vectors in the plane of the section (in $m \cdot s^{-1}$, vector scale shown at bottom right)

Figure 7.7(a) depicts the potential temperature, vertical velocity, and wind field in the $y-z$ plane. The Kelvin–Hemholtz billows characteristic of the interface between the density current and the ambient atmosphere are apparent, as is the enhanced vertical motion and return flow associated with the density current.

Figure 7.7(b) illustrates the simulation of the plume only. The plume is initiated by a heat source centered at $y=2{,}700$ m, the spatial configuration of which is a smoothed top-hat function. Characteristic features of the plume are similar to those described in more detail in the simulations by Cunningham et al. (2005).

The simulation in which both the plume and the density current are present is depicted in Fig. 7.7(c). It is evident that the interaction between the density current and the plume results in an apparent intensification of the plume, particularly in the vertical velocity field, in conjunction with the arrival of the circulation associated with the current, and that this intensification occurs before the head of the density current reaches the heat source. The intensification apparently occurs in response to the pressure perturbation that precedes the head of the current: this

pressure perturbation, which can impact the plume for a period of time before the arrival of the colder, more dense air behind the head of the current, counteracts the ambient flow at low levels such that the plume becomes more vertical (compare Fig. 7.7(b) with Fig. 7.7(c)), resulting in vertical velocities that are significantly stronger than those seen in the plume in isolation.

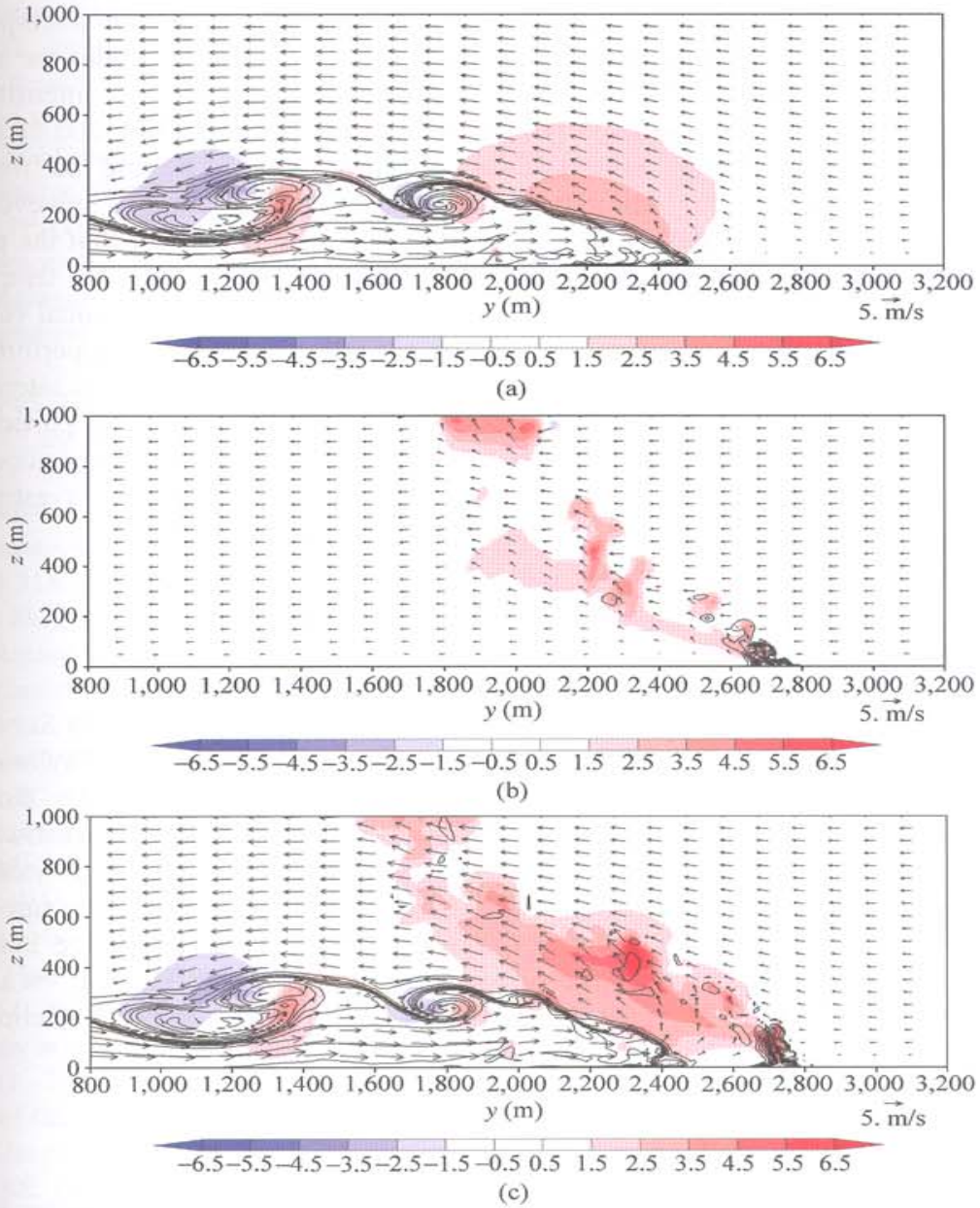

Figure 7.7 Vertical velocity (in $m \cdot s^{-1}$, shaded as indicated) and potential temperature (contour interval 1 K) in the $y-z$ plane for (a) the density current only, (b) the plume only, and (c) the density current and the plume. Vectors depict velocity in the plane of the section, with the scale in $m \cdot s^{-1}$ at the bottom right

7.5 Summary and Conclusions

Sea-breeze circulations are frequently observed to have a significant impact on fire behavior; however, the nature of the interaction between wildfires and the sea-breeze is poorly understood, and has not been studied extensively. In this Chapter, radar observations of a plume associated with a wildfire in Florida were presented that suggest that the arrival of a sea-breeze front results in a temporary, but significant, increase in fire intensity. This intensification precedes the arrival of the sea-breeze front at the location of the fire, such that the fire intensity is a maximum at the time of, and slightly after, the passage of the front, and decreases gradually thereafter with the arrival of cooler and moister air behind the front.

There is insufficient evidence to explain this intensification; however, the idealized numerical simulations presented in Section 7.4 suggest that the period of interaction preceding the arrival of the current may result in the temporary intensification of vertical velocity in the plume. This increase in vertical velocity appears to result from the interaction of the plume with a pressure perturbation that precedes the head of the density current. The direct impact of this interaction on fire behavior is uncertain, however, and requires further study, particularly using coupled atmosphere-fire models to explore the details of this interaction. Another aspect of the wildland fire-sea-breeze system that warrants investigation is how these interactions influence local and regional air quality.

Acknowledgements

The authors gratefully acknowledge Pam Brown of the USDA Forest Service in Tallahassee for providing the RAWS data for this study, and Scott Taylor of the Florida Division of Forestry for creating Fig. 7.1. We also thank Dr. Rodman Linn for insightful discussions on various aspects of the Chapter. DEH acknowledges support from the Florida Department of Agriculture and Consumer Services. PC acknowledges support from the USDA Forest Service, via a cooperative agreement between the Florida State University and the USDA Forest Service Southern Research Station, and from the FSU School of Computational Science, via a grant of resources on the IBM SP Series 690 Power4-based supercomputer "Eclipse".

References

Atkins NT, Wakimoto RM, (1997), Influence of the synoptic-scale flow on sea breezes observed during CaPE. *Mon. Wea. Rev.*, **125**: 2112 – 2130

Atkins NT, Wakimoto RM, Weckwerth TM, (1995), Observations of the sea-breeze front during CaPE. Part II: Dual-Doppler and aircraft analysis. *Mon. Wea. Rev.*, **123**: 944 – 969

Atlas D, (1960), Radar detection of the sea breeze. *J. Meteor.*, **17**: 244 – 258

Banta RM, Olivier LD, Holloway ET, Kropfli RA, Bartram BW, Crupp RE, Post MJ, (1992), Smoke-column observations from two forest fires using Doppler lidar and Doppler radar. *J. Appl. Meteor.*, **31**: 1328 – 1349

Battan LJ, (1973), Radar Observation of the Atmosphere. University of Chicago Press, 324

Clark TL, Jenkins MA, Coen JL, Packham DR, (1996a), A coupled atmosphere–fire model: Convective feedback on fire line dynamaics. *J. Appl. Meteor.*, **35**: 875 – 901

Clark TL, Jenkins MA, Coen JL, Packham DR, (1996b), A coupled atmosphere–fire model: Role of the convective Froude number and dynamic fingering at the fire line. *Int. J. Wildland Fire*, **6**: 177 – 190

Clark TL., Coen JL, Latham D, (2004), Description of a coupled atmosphere–fire model. *Int. J. Wildland Fire*, **13**: 49 – 63

Colby FP, (2004), Simulation of the New England Sea Breeze: The effect of grid spacing. *Wea. Forecasting*, **19**: 277 – 285

Cunningham P, Goodrick SL, Hussaini MY, Linn RR, (2005), Coherent vortical structures in numerical simulations of buoyant plumes from wildland fires. *Int. J. Wildland Fire*, **14**: 61 – 75

Dailey PS, Fovell RG, (1999), Numerical simulation of the interaction between the sea-breeze front and horizontal convective rolls. Part I: Offshore ambient flow. *Mon. Wea. Rev.*, **127**: 858 – 878

Droegemeier KK, Wilhelmson RB, (1987), Numerical simulation of thunderstorm outflow dynamics. Part I: Outflow sensitivity experiments and turbulence dynamics. *J. Atmos. Sci.*, **44**: 1180 – 1210

Fisher EL, (1960), An observational study of the sea breeze. *J. Meteor.*, **17**: 645 – 660

Fleischmann CM, McGrattan KB, (1999), Numerical and experimental gravity currents related to backdrafts. *Fire Safety J.*, **33**: 21 – 34

Fovell RG, (2005), Convective initiation ahead of the sea-breeze front. *Mon. Wea. Rev.*, **133**: 264 – 278

Fovell RG, Dailey PS, (2001), Numerical simulation of the interaction between the sea-breeze front and horizontal convective rolls. Part II: Alongshore ambient flow. *Mon. Wea. Rev.*, **129**: 2057 – 2072

Härtel C, Meiburg E, Necker F, (2000a), Analysis and direct numerical simulation of the flow at a gravity-current head. Part 1. Flow topology and front speed for slip and no-slip boundaries. *J. Fluid Mech.*, **418**: 189 – 212

Härtel C, Carlsson F, Thunblom M, (2000b), Analysis and direct numerical simulation of the flow at a gravity-current head. Part 2. The lobe-and-cleft instability. *J. Fluid Mech.*, **418**: 213 – 229

Hufford GL, Kelley HL, Sparkman W, Moore RK, (1998), Use of real-time multisatellite and radar data to support forest fire management. *Wea. Forecasting*, **13**: 592 – 605

Linn RR, (1997), A transport model for prediction of wildfire behavior. Scientific Report LA-13334-T, Los Alamos National Laboratory, 195

Linn RR, Cunningham P, (2005), Numerical simulations of grass fires using a coupled atmosphere–fire model: Basic fire behavior and dependence on wind speed. *J. Geophys. Res.*, in press

Linn RR, Reisner JM, Colman JJ, Winterkamp J, (2002), Studying wildfire behavior using FIRETEC. *Int. J. Wildland Fire*, **11**: 233 – 246

Özgökmen TM, Fisher PF, Dian J, Iliescu T, (2004), Three-dimensional turbulent bottom density currents from a high-order nonhydrostatic spectral element model. *J. Phys. Oceanogr.*, **34**: 2006 – 2026

Pielke RA, (1974), A three-dimensional numerical model of the sea breezes over south Florida. *Mon. Wea. Rev.*, **102**: 115 – 139

Rao PA, Fuelberg HE, Droegemeier KK, (1999), High-resolution modeling of the Cape Canaveral area land–water circulations and associated features. *Mon. Wea. Rev.*, **127**: 1808 – 1821

Rogers RR, Brown WOJ, (1997), Radar observations of a major industrial fire. Bull. *Amer. Meteor. Soc.*, **78**: 803 – 814

Sha W, Kawamura T, Ueda H, (1991), A numerical study on sea/land breezes as a gravity current: Kelvin–Helmholtz billows and inland penetration of the sea-breeze front. *J. Atmos. Sci.*, **48**: 1649 – 1665

Simpson JE, (1994), Sea Breeze and Local Winds. Cambridge University Press, 234

Simpson JE, Mansfield DA, Milford JR, (1977), Inland penetration of sea-breeze fronts. *Quart. J. Roy. Meteor. Soc.*, **103**: 47–76

Skamarock WC, Klemp JB, Dudhia J, (2001), Prototypes for the WRF (Weather Research and Forecasting) model. Preprints, Ninth Conf. On Mesoscale Processes, Fort Lauderdale, FL, *Amer. Meteor. Soc.*, J11 – J15

Wakimoto RM, (1982), The life cycle of thunderstorm gust fronts as viewed with Doppler radar and rawinsonde data. *Mon. Wea. Rev.*, **110**: 1060 – 1082

Wakimoto RM, Atkins NT, (1994), Observations of the sea-breeze front during CaPE. Part I: Single-Doppler, satellite, and cloud photogrammetry analysis. *Mon. Wea. Rev.*, **122**: 1092 – 1114

Wilson JW, Weckwerth TM, Vivekanandan J, Wakimoto RM, Russell RW, (1994), Boundary layer clear-air radar echoes: Origin of echoes and accuracy of derived winds. *J. Atmos. Oceanic. Technol.*, **11**: 1184 – 1206

Xu Q, Xue M, Droegemeier KK, (1996), Numerical simulations of density currents in sheared environments within a vertically confined channel. *J. Atmos. Sci.*, **53**: 770 – 786

Xue M, Xu Q, Droegemeier KK, (1997), A theoretical and numerical study of density currents in nonconstant shear flows. *J. Atmos. Sci.*, **54**: 1998 – 2019